

Structure-Based Redesign of a Methanol Oxidase into an “Aryl Alcohol Oxidase” for Enzymatic Synthesis of Aromatic Flavor Compounds

Wu, Bin; Wang, Shiyu; Ma, Yunjian; Yuan, Shuguang; Hollmann, Frank; Wang, Yonghua

DOI

[10.1021/acs.jafc.3c01069](https://doi.org/10.1021/acs.jafc.3c01069)

Publication date

2023

Document Version

Final published version

Published in

Journal of Agricultural and Food Chemistry

Citation (APA)

Wu, B., Wang, S., Ma, Y., Yuan, S., Hollmann, F., & Wang, Y. (2023). Structure-Based Redesign of a Methanol Oxidase into an “Aryl Alcohol Oxidase” for Enzymatic Synthesis of Aromatic Flavor Compounds. *Journal of Agricultural and Food Chemistry*, 71(16), 6406-6414. <https://doi.org/10.1021/acs.jafc.3c01069>

Important note

To cite this publication, please use the final published version (if applicable). Please check the document version above.

Copyright

Other than for strictly personal use, it is not permitted to download, forward or distribute the text or part of it, without the consent of the author(s) and/or copyright holder(s), unless the work is under an open content license such as Creative Commons.

Takedown policy

Please contact us and provide details if you believe this document breaches copyrights. We will remove access to the work immediately and investigate your claim.

Green Open Access added to TU Delft Institutional Repository

'You share, we take care!' - Taverne project

<https://www.openaccess.nl/en/you-share-we-take-care>

Otherwise as indicated in the copyright section: the publisher is the copyright holder of this work and the author uses the Dutch legislation to make this work public.

Structure-Based Redesign of a Methanol Oxidase into an “Aryl Alcohol Oxidase” for Enzymatic Synthesis of Aromatic Flavor Compounds

Bin Wu, Shiyu Wang, Yunjian Ma,* Shuguang Yuan, Frank Hollmann,* and Yonghua Wang*



Cite This: *J. Agric. Food Chem.* 2023, 71, 6406–6414



Read Online

ACCESS |



Metrics & More



Article Recommendations



Supporting Information

ABSTRACT: Alcohol oxidases (AOxs) catalyze the aerobic oxidation of alcohols to the corresponding carbonyl products (aldehydes or ketones), producing only H₂O₂ as the byproduct. The majority of known AOxs, however, have a strong preference for small, primary alcohols, limiting their broad applicability, e.g., in the food industry. To broaden the product scope of AOxs, we performed structure-guided enzyme engineering of a methanol oxidase from *Phanerochaete chrysosporium* (PcAOx). The substrate preference was extended from methanol to a broad range of benzylic alcohols by modifying the substrate binding pocket. A mutant (PcAOx-EFMH) with four substitutions exhibited improved catalytic activity toward benzyl alcohols with increased conversion and *k*_{cat} toward the benzyl alcohol from 11.3 to 88.9% and from 0.5 to 2.6 s⁻¹, respectively. The molecular basis for the change of substrate selectivity was analyzed by molecular simulation.

KEYWORDS: alcohol oxidase, molecular modification, substrate selectivity, flavor compounds

1. INTRODUCTION

Flavor compounds are central to the food industry.^{1,2} The demand for natural flavor compounds^{3,4} is continuously growing due to an increasing customer demand for “natural” products. Benzaldehyde derivatives are important components of the flavor and fragrance industry. Benzaldehyde itself has a bitter almond-like scent and is commonly used to create artificial almond, cherry, and other fruit flavors.⁵ Also, benzaldehyde derivatives have a wide range of aromatic profiles and are therefore more widely used in perfumery and flavoring. Vanillin, for example, is widely used as a flavoring agent in food, beverages, and pharmaceutical products.⁶ It is also used as a fragrance component in personal care products, perfumes, and candles. Other important natural aldehydes are, for example, cinnamic aldehyde, which has a spicy cinnamon-like aroma and is used in flavorings, fragrances, and personal care products;⁷ heliotropin, which has a sweet, powdery vanilla-like aroma and is used in fragrances and air fresheners;⁸ and anisaldehyde, which has a sweet, anise-like aroma and is used in fragrances and flavorings.⁹

Overall, benzaldehyde derivatives play an important role in the flavor and fragrance industry,¹⁰ providing a wide range of aromatic profiles that are used to create unique and appealing scents and flavors in a variety of consumer products. Although various synthetic routes for aromatic aldehydes and ketones exist,¹¹ enzymatic synthesis routes are highly desirable as the products obtained from those are considered natural.^{1,3,4}

In the past few years, aryl alcohol oxidases (AAOx, EC 1.1.3.7) have gained considerable interest as catalysts for the selective and mild oxidation of benzyl alcohols to the corresponding aldehydes.^{12,13} The recombinant expression of functional fungal enzymes in prokaryotic hosts such as *Escherichia coli*, however, still is challenging due to the lack

of post-translational modifications such as glycosylation, etc.^{14–18} Therefore, it is critical to find alternative catalysts to aromatic alcohol oxidase. Alcohol oxidases (AOx, E.C. 1.1.3.13) are viable alternatives to the above-mentioned AAOx. As members of the so-called glucose–methanol–choline (GMC) superfamily of oxidoreductases, AOx catalyzes the aerobic (H₂O₂-forming) oxidation of primary alcohols.¹⁹ However, their substrate scope appears to be largely limited to smaller and primary alcohols.^{20,21} Particularly, the alcohol oxidase from *Phanerochaete chrysosporium* (PcAOx, GenBank: HG425201, UniProtKB/TrEMBL:T2M2J4) is an interesting enzyme due to its high recombinant expression level in *E. coli* (more than 600 mg × L⁻¹ fermentation broth⁻¹) and its simple, one-step purification.^{22,23} Notably, PcAOx exhibits only a limited ability to oxidize sterically more demanding starting materials such as benzylic alcohols.²⁴ To extend the substrate scope of PcAOx, we set out to perform structure-guided engineering of this enzyme.

2. MATERIALS AND METHODS

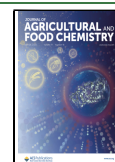
2.1. Chemical Reagents and Materials. All chemicals were purchased from Sigma-Aldrich (St. Louis, MO 63103), TCI (Tokyo, Japan), Acros (New Jersey), or Aladdin (Shanghai, China) with the highest purity available and used without further treatment. *E. coli* BL21 (DE3) was used for the production of the biocatalyst, and *E. coli*

Received: February 20, 2023

Revised: March 30, 2023

Accepted: April 3, 2023

Published: April 11, 2023



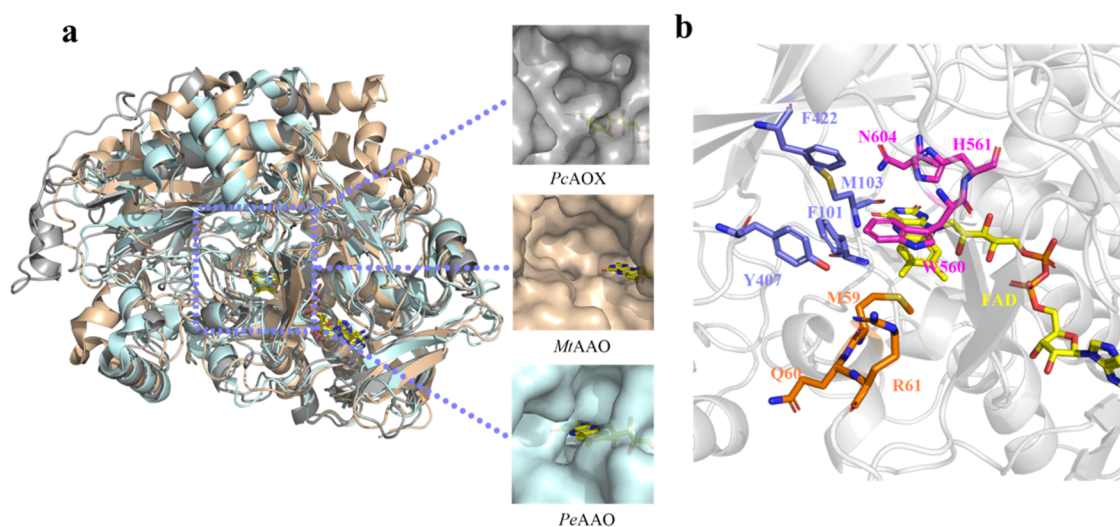


Figure 1. Structural analysis of PcAOx. (a) Structure comparison of PcAOx with MtAAOx and PeAAOx. PcAOx (PDB ID: 6H3G) shown in gray, MtAAOx (PDB ID: 6O9N) shown in light brown, and PeAAOx (PDB ID: SOCI) in light blue. (b) PcAOx key sites for catalytic properties. Yellow, FAD; rose red, bottom of the active center; blue, wall of catalytic cavity; brown, top of the catalytic pocket.

TOP10 was used for constructing PcAOx and its mutants. Water was purified with a Millipore (Bedford, MA) Milli-Q water system.

2.2. Expression and Preparation of PcAOx and Mutants.

The codon-optimized PcAOx-encoding gene (Genbank: HG425201.1) was synthesized by Shanghai Shengong Biotechnology Co., LTD., and cloned in expression vector pET28a (+) into the *EcoR* I/*Sal* I site. The constructed pET28a-PcAOx was transformed into *E. coli* BL21 (DE3) for expression. The complete gene sequence and amino acid sequence are shown in Table S1 (Supporting Information). The sequences of PcAOx and its mutant were submitted to the NCBI database with the accession numbers OP503494.1 and OP503495.1.

The pET28a-PcAOx plasmid was used as the template for mutant construction. The online quick change primer design website (<https://www.agilent.com.cn/store/primerDesignProgram.jsp>) was used for the mutant primer design, and the specific mutation sites and primer sequences are shown in Tables S2 and S3. Transformed *E. coli* BL21 (DE3) cells were cultured to an OD_{600} of 0.7–0.8 in 5 mL of LB medium containing $50 \mu\text{g mL}^{-1}$ kanamycin at 37°C and 220 rpm. Then, the cells were inoculated to 500 mL of TB medium containing 1% glucose and cultured at 37°C until $OD_{600} \approx 0.8$ –0.9 and induced at 20°C with 0.5 mM IPTG (isopropyl- β -D-thiogalactoside, BBI Life Sciences Corporation) for 20 h. The cells were collected by centrifugation for 30 min ($5500g$, 4°C) and stored at -80°C .

Cells were resuspended in lysis buffer (50 mM potassium phosphate pH 7.5, 400 mM NaCl, 100 mM KCl, 40 mM imidazole) and were ultrasonically broken on ice for 20 min. The ultrasonic pulsed on-time and off-time were 2 and 2 s, respectively. The cell extract was centrifuged at 4°C , $11,000g$ for 30 min, and the supernatant was loaded to a Ni column (prebalanced with lysis buffer). An imidazole gradient of 40–500 mM was used to elute the enzyme. Active fractions were collected and desalted. SDS-PAGE was used to show the enzyme purity. Pure protein was stored at -80°C until further use. SDS-PAGE results of the wild type and mutants are shown in Figures S1 and S2. In addition, the expression quantities of the wild type and mutants are shown in Table S4.

2.3. Enzyme Assays. Hydrogen peroxide (H_2O_2) was generated using AOX upon oxidation of a substrate and monitored in time using horseradish peroxidase (HRP) (40 mg L^{-1}). Here, 4-amino-antipyrine and dichloro-2-hydroxybenzenesulfonic acid were used to produce a pink-purple quinone. The absorption at 515 nm was monitored using an Infinite M200 Pro plate reader (TECAN). About 500 μL of H_2O_2 solution with concentration gradients of 0.01, 0.02, 0.04, 0.06, 0.08, 0.1, 0.12, and 0.15 mM and 50 μL of a standard solution of each

concentration were put into the 96-well plate. The solution, containing 50 μL of reaction solution (1 mM 4-amino-antipyrine, 2 mM dichloro-2-hydroxybenzenesulfonic acid) and 100 μL of buffer solution (50 mM PBS pH 7.5), was added; then, the absorbance value was measured at 515 nm after 15 min. There were three parallel groups for each experiment. Finally, the standard curve was drawn with the concentration of H_2O_2 as the X-axis and the absorption value as the Y-axis to calculate the enzyme activity.

The kinetic constants were determined by GC analysis. The solution (1 mL), containing different concentrations of the substrates (0.5, 0.8, 1.0, 1.5, 2, 3, 5, 10, 20, 30, 50 mM), buffer (pH 7.5 50 mM phosphate), and 10 μM enzyme, was added into 5 mL glass bottles for reaction (30°C and 500 rpm). The solution of HCl (3 M, 1 mL) was added to terminate the reaction. Ethyl acetate (1 mL) was added for extraction. After centrifugation, the upper sample was placed in a brown bottle for GC detection. The blank group was added with an equal volume of boiled enzyme, and all experiments were conducted in three parallel groups.

2.4. Substrate Preference Assays. The catalytic reaction was carried out in a 4 mL reaction flask with a total reaction system of 1 mL. The reaction was carried out at pH 8.0, 30°C , 500 rpm, containing 25 μM enzyme and 25 mM substrate (dissolved using 5% DMSO). Gas chromatography for product detection was performed on an Agilent 7890B GC system (Agilent Technologies, Palo Alto, CA) outfitted with an HP-5 column (30 m length \times 0.32 mm I.D. \times 0.25 μm film thickness) with an FID detector. The heating procedure was as follows: inlet temperature, 280°C ; detector temperature, 280°C ; initial temperature of the column, 50°C for 2 min, then increased to 150°C for 3 min at 8°C min^{-1} , and then to 280°C at $15^\circ\text{C min}^{-1}$, and maintained for 10 min. Retention time of various compounds is shown in Table S5.

2.5. Molecular Dynamics (MD) Simulations. The structure of the mutant PcAOx-EFMH was manually constructed from wild-type PcAOx (PDB ID: 6H3G) followed by a short energy minimization via Schrodinger, 2018. Benzyl alcohol was manually moved into the catalytic pocket as the specific pose. Actually, manual insertion, docking, Monte Carlo dynamics, and/or conformation-searching techniques can also be used to construct the initial complex structures. Here, the binding pose of benzyl alcohol in the catalytic pocket is already known.²⁵ Therefore, we constructed the complexes manually. Molecular dynamic simulation was performed using Gromacs 2020²⁶ with the Amber FF99SB force field for protein and the GAFF2 force field for ligands. Structure optimization and charge calculation of small molecules were performed at the AM1-BCC level using sqm software. The complex systems were solvated in

a 1.5 nm TIP3P water box. NaCl (0.15 M) was added to neutralize the system. The molecular dynamic simulation included a short energy minimization, 300 ps simulation with constant temperature and constant volume condition, 400 ps simulation with constant temperature and constant pressure condition, and 10 ns production simulation. Metadynamics was performed to simulate the process of substance binding from solution to the catalysis pocket by Gromacs 2020 and plumed 2.6.²⁷ The widths and heights of the Gaussian hills were set to 0.1 and 1.0, respectively. The bias factor was set to 5. Binding free energy prediction and decomposition were performed using gmx_MMPBSA V1.4.3²⁸ with the GB^{OBC2} model.²⁹

3. RESULTS AND DISCUSSION

3.1. Key Sites Selected by Structural Comparative Analysis of PcAOx and AAOxs. Two AAOxs (from

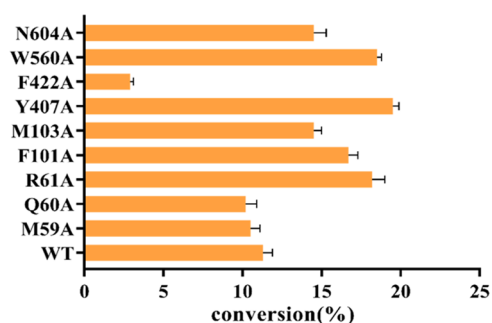


Figure 2. Alanine scan results of PcAOx. (Reaction conditions: 25 μ M purified enzyme, 50 mM benzyl alcohol, pH 7.5 buffer (50 mM PBS) were mixed and stirred at 500 rpm at 30 °C in a total volume of 1 mL for 24 h).

Thermothelomyces thermophilus M77 and *Pleurotus eryngii*, MtAAO and PeAAO) have been reported to exhibit high catalytic activity on aromatic alcohols.^{30,31} We therefore compared the active site architecture of these two enzymes with that of PcAOx (Figure 1). While the catalytic FADs in MtAAO and PeAAO are readily accessible, the FAD within PcAOx is completely wrapped. Especially W560, N604, F101, M103, Y407, F422, M59, Q60, and R61 are located in close vicinity of the flavin cofactor, thereby imposing a significant steric constraint (Figure 1). We therefore speculated that these amino acid residues may impede the binding of, e.g., benzyl alcohol in a productive conformation to the FAD prosthetic group.

3.2. Mutant Design and Characterization Based on Amino Acid Properties. Based on the structural analysis, we chose the aforementioned amino acids for an alanine scan. Indeed, PcAOx mutants R61A, F101A, M103A, Y407A, W560A, and N604A showed modestly increased benzyl alcohol oxidation rates compared to the wild-type enzyme (Figure 2). For the following amino acid exchanges, we chose Gly, Leu, Phe as well as Ser and Asn to cover a broader range of steric demand and polarity. As position 604 (here N604) within AAOx is a highly conserved His, we also constructed N604H as well as N604F and N604R (as controls).

Interestingly, PcAOx-R61E mutants exhibiting further mutations at F101 and M103 showed only decreased activity compared to their parent (R61E) and therefore were discarded. Currently, we are lacking a plausible explanation for this observation. Further studies such as obtaining crystal structures of all mutants investigating this will be necessary.

Starting with R61, we generated the following mutants: R61G, R61N, R61S, R61E, and R61D. R61E showed a 33%

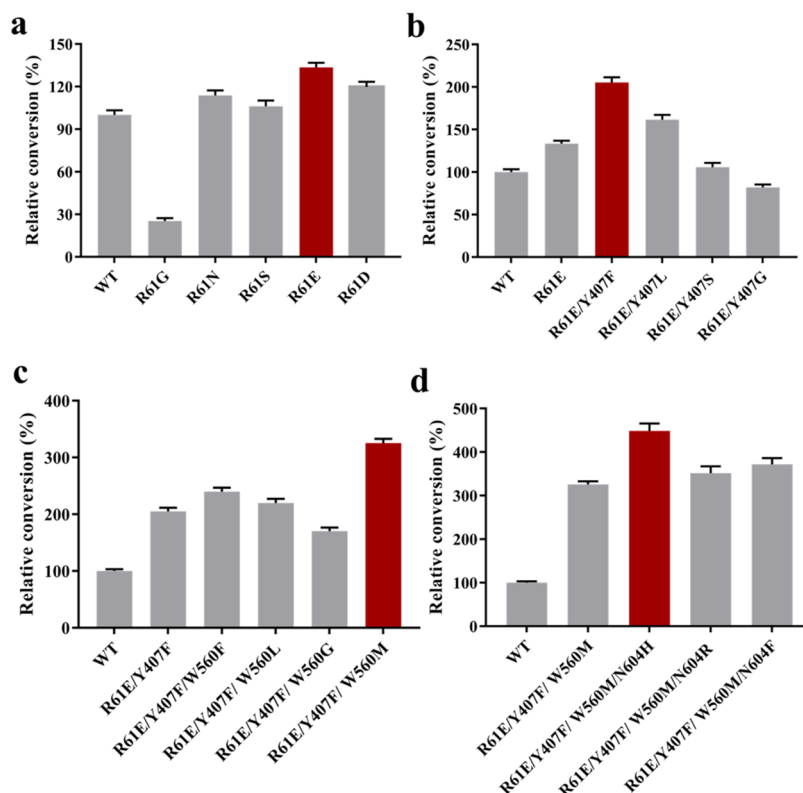


Figure 3. Conversion of benzyl alcohol catalyzed by multisite superimposed mutants. (a) Site R61, (b) site R61 superimposed site Y407, (c) site R61 superimposed sites Y407 and W560, and (d) site R61 superimposed sites Y407, W560, and N604.

Table 1. Conversion of PcAOX and Its Mutants with Series Substrates^a

Substrate	Product	Conversion (%)				
		WT	R61E	R61E/Y407F	R61E/Y407F/W560M	R61E/Y407F/W560M/N604H
benzyl alcohol	benzaldehyde	11.3 ±0.6	15.2 ±1.1	50.3 ±3.2	64.2 ±2.4	88.9 ±3.3
R-1-benzene ethanol	acetophenone	1.4 ±0.1	2.1 ±0.1	2.6 ±0.1	3.4 ±0.2	1.7 ±0.1
S-1-benzene ethanol	acetophenone	11.5 ±0.9	18.2 ±1.7	42.8 ±2.6	65.7 ±2.7	75.3 ±3.2
2-phenylethanol	acetophenone	0.6 ±0.2	10.2 ±1.5	16.2 ±1.9	28.5 ±3.5	45.3 ±2.6
1-phenylpropanol	1-phenylacetone	n.d.	6.5 ±0.9	10.5 ±0.9	16.4 ±2.6	26.4 ±2.1
3-phenylpropanol	phenylpropionaldehyde	1.9 ±0.9	9.2 ±0.5	15.6 ±1.9	40.4 ±3.1	64.4 ±1.6
4-methylbenzyl alcohol	4-methylbenzaldehyde	15.6 ±0.7	29.3 ±2.2	42.5 ±3.7	59.6 ±2.0	89.9 ±4.3
4-aminobenzyl alcohol	4-aminobenzaldehyde	11.6 ±0.4	15.2 ±1.3	17.5 ±1.1	21.6 ±2.4	48.0 ±3.6
4-hydroxybenzyl alcohol	4-hydroxybenzaldehyde	13.7 ±0.7	15.9 ±1.2	59.3 ±2.9	55.7 ±2.8	78.0 ±2.3
4-methoxybenzyl alcohol	4-methoxybenzaldehyde	32.3 ±2.2	40.2 ±2.9	50.4 ±2.8	56.8 ±3.7	86.0 ±3.3
1-Naphthalenemethanol	1-Naphthalenaldehyde	2.3 ±0.6	5.3 ±0.5	11.6 ±1.5	26.3 ±3.5	39.8 ±4.5
2-Naphthalenemethanol	2-Naphthalenaldehyde	2.4 ±0.5	5.8 ±0.5	12.6 ±2.5	29.0 ±2.5	38.7 ±5.9

^aReaction conditions: 25 μ M enzyme, 25 mM substrate (dissolved using 5% DMSO), pH 8.0, 30 °C.

increased conversion of benzyl alcohol (Figure 3a), which is why we chose it as the parent for the mutagenesis in position Y407. To relax the steric demand in this position, we generated the mutants Y407F, Y407L, Y407S, and Y407G. The mutation Y407F (Figure 3b) resulted in significant activity improvements of 54% conversion of benzyl alcohol compared to the parent R61E mutant. To generate even more space around the

prosthetic group mutants W560F, W560L, W560G, and W560M were evaluated (using mutant R61E-Y407F as the template). In this round of mutagenesis, W560F performed the best with another 17% improvement in conversion over its direct parent (Figure 3c). Finally, using R61E-Y407F-W560M as the parent, we mutated N604 to a histidine to reconstitute the His–His motif that is highly conserved in AAoxs.³² Indeed,

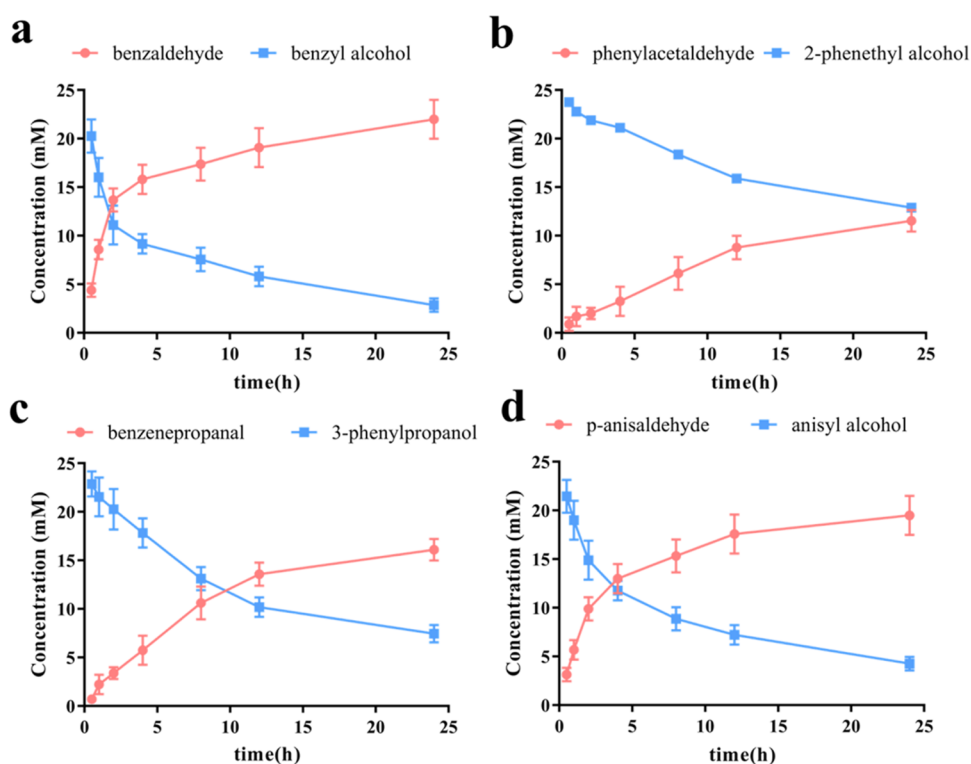


Figure 4. Representative time-courses of *PcAOX*-EFMH-catalyzed oxidation of benzyl alcohol (a), 2-phenyl ethanol (b), 3-phenylpropanol (c), and anisyl alcohol (d). Reaction conditions: 25 μ M enzyme, 25 mM substrate (dissolved using 5% DMSO), pH 8.0, 30 $^{\circ}$ C, 500 rpm.

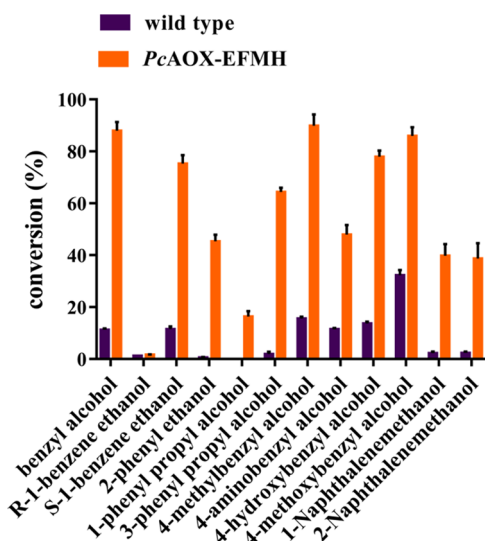


Figure 5. Conversion of a series of alcohols catalyzed by the mutant *PcAOX*-EFMH.

this substitution resulted in further improvement of the catalytic activity (Figure 3d).

Overall, the quadruple mutant *PcAOX*-R61E-Y407F-W560M-N604H (*PcAOX*-EFMH) displayed a significantly improved 8-fold conversion of benzyl alcohol to benzaldehyde compared to the wild-type enzyme.

3.3. Exploring the Substrate Scope. We further explored the catalytic activity of the mutant *PcAOX*s generated toward a broader range of primary and secondary alcohols (Table 1). The general trend observed with benzyl alcohol as the starting material could be reproduced with the further starting materials tested (Table 1). In the case of secondary

alcohols such as 1-phenyl ethanol also the stereoselectivity toward the (*S*)-enantiomer was increased. All mutants exhibited strict (*S*)-selectivity.

We further determined the kinetic parameters of both wt-*PcAOx* and *PcAOx*-EFMH for some small alcohols such as methanol and ethanol as well as sterically more demanding benzyl alcohols. *PcAOx*-EFMH entirely lost its catalytic activity on methanol and ethanol. At the same time, both the affinity and catalytic activity toward benzyl alcohol increased. Overall, the catalytic efficiency in terms of k_{cat}/K_M increased more than 60-fold from 12 $\text{M}^{-1} \text{s}^{-1}$ for wt-*PcAOx* to 795 $\text{M}^{-1} \text{s}^{-1}$ for *PcAOx*-EFMH.

Some representative time-courses of *PcAOx*-EFMH-catalyzed alcohol oxidations are shown in Figure 4. In most cases, the reaction rate decreased significantly after approx. 12 h of reaction time, which may be caused by enzyme inactivation. Indeed, around 12 h, we observed a precipitate in the reaction mixture. Right now, we cannot fully explain this, but it appears likely that either hydrogen peroxide accumulating as a stoichiometric byproduct or the reactive aldehyde product may negatively influence the enzyme stability. Further experiments investigating this are currently underway as well as suitable reaction engineering solutions (such as catalase addition to dismutate H_2O_2 and/or in situ product removal to alleviate possible aldehyde-borne inactivation). The change of substrate selectivity of the mutant was found in the substrate spectra of the mutant and the wild type (Figure 5).

3.4. Molecular Simulation on the Differences between wt-*PcAOx* and *PcAOx*-EFMH in Substrate Scope. In order to gain a deeper understating of the molecular reason for the change of substrate selectivity of *PcAOX*, molecular dynamics simulation was used. The conformational root-mean-square deviation (RMSD), the distance between

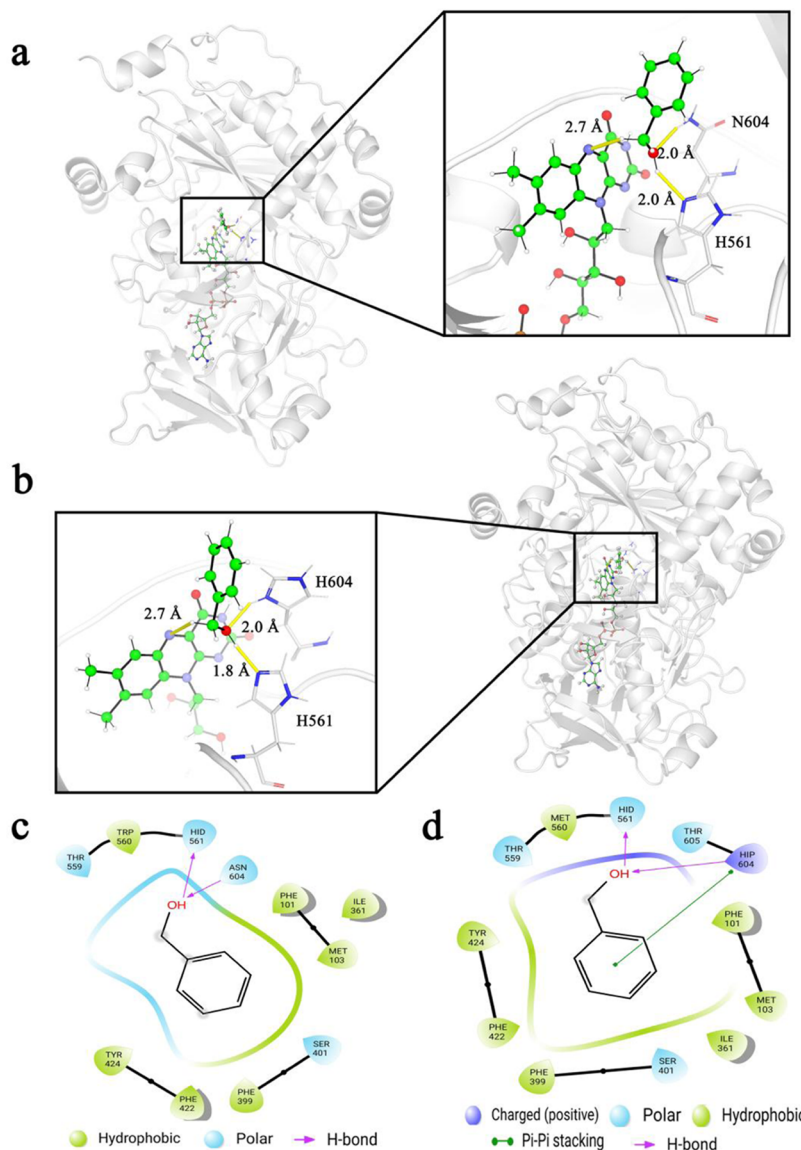


Figure 6. Binding results of benzyl alcohol with the wild type and mutant. (a) Binding of benzyl alcohol and *PcAOx*-FAD. (b) Binding of benzyl alcohol and *PcAOx*-EFMH-FAD. (c) Interaction of benzyl alcohol and *PcAOx*-FAD. (d) Interaction of benzyl alcohol and *PcAOx*-EFMH-FAD.

Table 2. Kinetic Parameters of Wild-Type and Mutant *PcAOx*-EFMH

enzyme	substrate	K_m (mM)	k_{cat} (s^{-1})	k_{cat}/K_m ($M^{-1} s^{-1}$)
wild type	methanol	1.5 ± 0.5	12.4 ± 0.6	8231
	ethanol	9.2 ± 2.2	12.3 ± 0.5	1334
	benzyl alcohol	35.8 ± 3.5	0.5 ± 0.1	12
<i>PcAOx</i> -EFMH	methanol	α	α	α
	ethanol	α	α	α
	benzyl alcohol	3.3 ± 0.5	2.6 ± 0.4	795
	2-phenyl ethanol	2.6 ± 0.3	1.7 ± 0.4	643
	3-phenyl ethanol	2.5 ± 0.4	1.3 ± 0.5	525

α The activity was too low to be detected.

Table 3. Binding Free Energy of Benzyl Alcohol Computed Using the MM/GBSA Method (in kcal mol $^{-1}$)

	ΔG	VDWAALS ^a	EEL ^b	EGB ^c	ESURF ^d
wild type	-24.0738	-16.4414	-21.3774	16.4775	-2.7325
R61E/Y407F/W560M/N604H	-28.2553	-16.3637	-29.9211	20.9323	-2.9028

^avan der Waals contribution. ^bElectrostatic contribution. ^cPolar contribution of solvation energy. ^dNonpolar contribution of solvation energy.

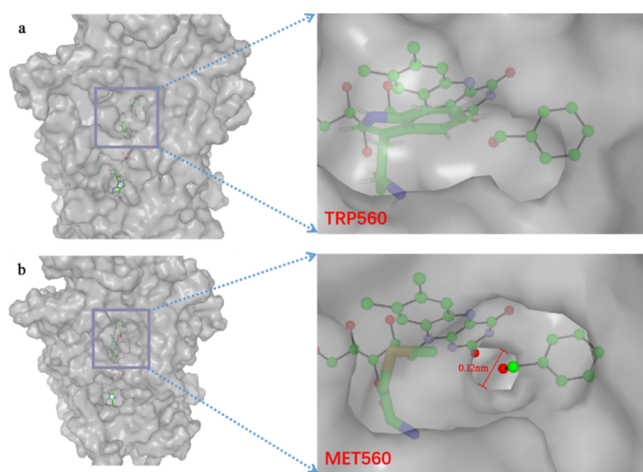


Figure 7. Comparison of the active site access channel for the *PcAOx*-benzyl alcohol complex for (a) wt-*PcAOx* and (b) *PcAOx*-EFMH.

benzyl alcohol and the atom N5 of FAD, the distance between benzyl alcohol and HIS561, and the distance between benzyl alcohol and ASN604 were firm (Figures S3 and S4). As a result, the simulations were convergent and bindings of benzyl alcohol were stable. Within *PcAOx*, the bound benzyl alcohol formed two hydrogen bonds with HIS561 (histidine with hydrogen on the delta nitrogen) and ASN604 (Figure 6a,c). In

the case of the *PcAOx*-EFMH system, an additional π - π interaction with HIP604 (histidine with hydrogens on both nitrogens) was observed (Figure 6b,d). This may, at least partially, explain the increasing affinity toward benzyl alcohol while moving from *PcAOx* to *PcAOx*-EFMH (Table 2).

According to the dynamic simulation trajectories from 8 ns to 10 ns, the MM/GBSA model was used to estimate the free energy of the benzyl alcohol bound to *PcAOx* and *PcAOx*-EFMH, respectively. As shown in Table 3, the binding free energy of the benzyl alcohol with the *PcAOx* wild type was -24.0738 kcal mol $^{-1}$, which was higher than the counterpart of the *PcAOx*-EFMH complex (-28.2553 kcal mol $^{-1}$), further indicating that the benzyl alcohol shows a higher affinity to *PcAOx*-EFMH. Furthermore, the interaction energy of benzyl alcohol with residues in the catalytic pocket was also calculated via the MM/GBSA model. As a result, the electrostatic attraction energy between the benzyl alcohol and the residue HIP604 in *PcAOx*-EFMH was -9.4154 kcal mol $^{-1}$, which was higher than that between the benzyl alcohol and the residue Asn604 in wild-type *PcAOx* (-3.833 kcal mol $^{-1}$), implying that the mutation N604H contributes to the improvement of *PcAOx* activity. Considering the structural information, the new π - π stacking interaction between the benzyl alcohol and the 604th residue contributes to the increase of electrostatic attraction, further increasing the affinity between *PcAOx* and its ligands.

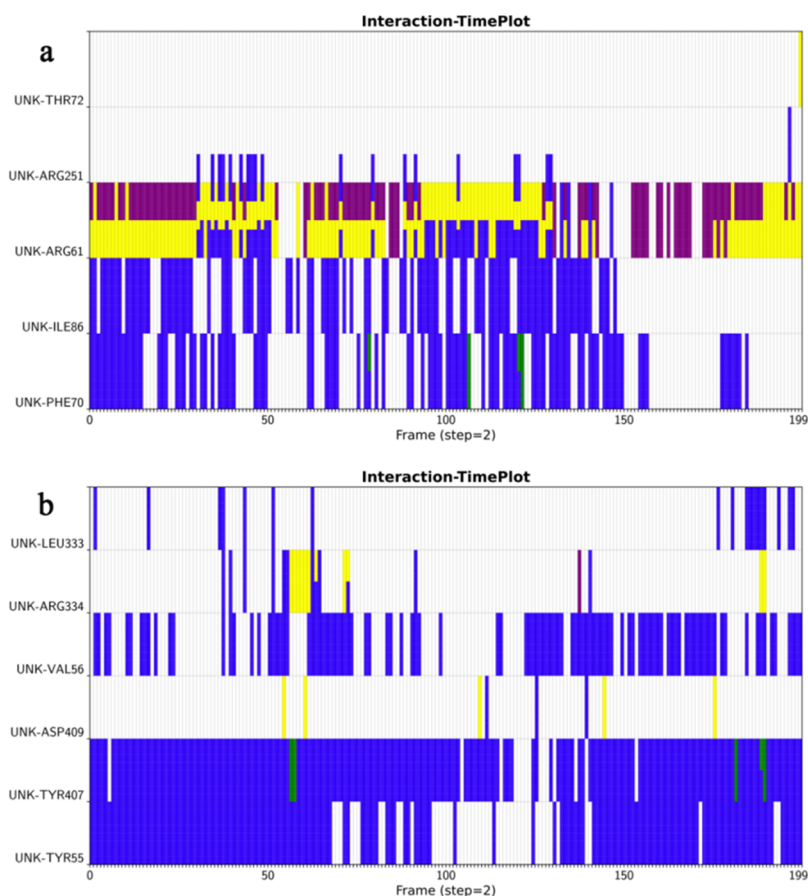


Figure 8. Statistics of interactions between *PcAOx* and benzyl alcohol. (a) Interactions between benzyl alcohol and Arg61. (b) Interactions between benzyl alcohol and Tyr407. Hydrophobic interactions, hydrogen bonds, cation- π , and π - π stack interactions are represented in blue, yellow, purple, and green, respectively. The y-axis represents which residues interact with benzyl alcohol. The frame in the x-axis indicates the time steps during the molecular dynamics.

Another important contribution was identified within the substrate access channel, which in the case of PcAOx-EFMH was shown to be considerably wider (substitution of tryptophane by the smaller methionine (W560M)), thereby exerting less steric resistance for reagent access to and from the active site (Figure 7).

To simulate the association and dissociation processes of the substrate and the enzyme, 100 ns metadynamics simulation was applied on the PcAOx-FAD-benzyl alcohol system. A distance of the N5 atom of the FAD and benzyl carbon atom was selected as the covariable. In addition to the binding of benzoic acid with the wild-type PcAOx at the covariable of 0.05–0.1 nm (Figure S5), other bindings occurred at the covariable of 0.15–0.2 nm. In other words, benzyl alcohol must cross the energy barrier at the covariable of 0.15–0.2 nm before binding to the catalytic site. Evidently, the appearance of this energy barrier reduced the catalytic efficiency. The trajectory of the metadynamic simulation was analyzed to ascertain the cause of the energy barrier. As a consequence, benzyl alcohol bound to the catalytic site and other sites, including the site near ARG61 and TYR407 (Figure 8a,b and Videos 1 and 2). Unfortunately, the binding of the benzyl alcohol to these two sites could not catalyze the chemical reaction. It lowers the energy barrier after the mutation.

In conclusion, with this contribution, we demonstrate the potential of alcohol oxidases to produce benzaldehydes in a “natural way.” Limitations of pre-existing wild-type enzymes such as narrow substrate scope can be addressed via structure-guided enzyme engineering. In this particular case, a well-expressed natural alcohol oxidase (wt-PcAOx) was improved for the selective and benign oxidation of simple benzyl alcohols. The engineered mutant (PcAOx-EFMH) combined a high expression level and high catalytic activity toward target starting materials, thereby constituting a promising starting point for preparative-scale transformations, which are currently ongoing in our laboratory.

■ ASSOCIATED CONTENT

SI Supporting Information

The Supporting Information is available free of charge at <https://pubs.acs.org/doi/10.1021/acs.jafc.3c01069>.

Purification results of alcohol oxidase PcAOx wild-type and mutants, RMSD of wild-type and mutants with benzyl alcohol, nucleotide, and amino acid sequences of PcAOx wild-type and mutant, primer list, protein expression level, and simulation results of interaction between mutant and benzyl alcohol (PDF)

Demonstration of substrate benzyl alcohol staying near R61 (Video S1) (MP4)

Demonstration of substrate benzyl alcohol staying near Y407 (Video S2) (MP4)

■ AUTHOR INFORMATION

Corresponding Authors

Yunjian Ma – School of Food Science and Engineering, South China University of Technology, Guangzhou 510640, China; Email: femayj@mail.scut.edu.cn

Frank Hollmann – Department of Biotechnology, Delft University of Technology, 2629HZ Delft, The Netherlands; orcid.org/0000-0003-4821-756X; Email: f.hollmann@tudelft.nl

Yonghua Wang – School of Food Science and Engineering, South China University of Technology, Guangzhou 510640, China; orcid.org/0000-0002-3255-752X; Email: yonghw@scut.edu.cn

Authors

Bin Wu – School of Bioscience and Bioengineering, South China University of Technology, Guangzhou 510006, China

Shiyu Wang – Research Center for Computer-Aided Drug Discovery, Shenzhen Institute of Advanced Technology, Chinese Academy of Sciences, Shenzhen 518055, China; College of Chemical Science, University of Chinese Academy of Sciences, Beijing 101408, China

Shuguang Yuan – Research Center for Computer-Aided Drug Discovery, Shenzhen Institute of Advanced Technology, Chinese Academy of Sciences, Shenzhen 518055, China

Complete contact information is available at:

<https://pubs.acs.org/10.1021/acs.jafc.3c01069>

Funding

This study was funded by the Key Realm R&D Program of Guangdong Province (grant number 2022B0202050003), the Key Program of Natural Science Foundation of China (grant number 31930084), and the work of Shuguang Yuan was supported by funding from the Chinese Academy of Sciences, the Shenzhen Institute of Advanced Technology, CAS, Shenzhen government (grant number JCYJ20200109114818703) as well as that from Guangdong province (grant number 2019QN01Y306). F.H. acknowledges funding from the European Union (ERC, PeroxyZyme, No 101054658). Views and opinions expressed are however those of the authors only and do not necessarily reflect those of the European Union or the European Research Council. Neither the European Union nor the granting authority can be held responsible for them.

Notes

The authors declare no competing financial interest.

■ ACKNOWLEDGMENTS

The authors sincerely thank Professor Marco W. Fraaije for his helpful comments and guidance on this work.

■ REFERENCES

- Wickramasinghe, P. C. K.; Munafo, J. P., Jr. Biosynthesis of Benzylic Derivatives in the Fermentation Broth of the Edible Mushroom, *Ischnoderma resinosa*. *J. Agric. Food Chem.* **2020**, *68*, 2485–2492.
- Krings, U.; Berger, R. G. Biotechnological Production of Flavours and Fragrances. *Appl. Microbiol. Biotechnol.* **1998**, *49*, 1–8.
- Perdomo, I. C.; Gianolio, S.; Pinto, A.; Romano, D.; Contente, M. L.; Paradisi, F.; Molinari, F. Efficient Enzymatic Preparation of Flavor Esters in Water. *J. Agric. Food Chem.* **2019**, *67*, 6517–6522.
- Bora, P. K.; Borah, G.; Kalita, D.; Saikia, S. P.; Haldar, S. Mushroom-Mediated Reductive Bioconversion of Aldehyde-Rich Essential Oils for Aroma Alteration: A Rose-like Floral Bioflavor from Citronella Oil. *J. Agric. Food Chem.* **2023**, *71*, 1690–1700.
- Martin, V.; Giorello, F.; Fariña, L.; Minteguiaga, M.; Salzman, V.; Boido, E.; Aguilar, P. S.; Gaggero, C.; Dellacassa, E.; Mas, A.; Carrau, F. De Novo Synthesis of Benzenoid Compounds by the Yeast *Hanseniaspora Vineae* Increases the Flavor Diversity of Wines. *J. Agric. Food Chem.* **2016**, *64*, 4574–4583.
- Horvat, M.; Fiume, G.; Fritsche, S.; Winkler, M. Discovery of Carboxylic Acid Reductase (CAR) from *Thermothelomyces*

Thermophila and Its Evaluation for Vanillin Synthesis. *J. Biotechnol.* **2019**, *304*, 44–51.

(7) Monteiro, A. B.; de Andrade, H. H. N.; Felipe, C. F. B.; de Almeida, R. N. Pharmacological Studies on Cinnamic Alcohol and Its Derivatives. *Rev. Bras. Farmacogn.* **2021**, *31*, 16–23.

(8) Yamagishi, R.; Yokomaku, A.; Omoto, F.; Misao, K.; Takada, K.; Yoshimatsu, S.; Abe, A.; Hayashi, M. Sleep-Improving Effects of the Aromatic Compound Heliotropin. *Sleep Biol. Rhythms* **2010**, *8*, 254–260.

(9) Han, D.; Kurusarttra, S.; Ryu, J.-Y.; Kanaly, R. A.; Hur, H.-G. Production of Natural Fragrance Aromatic Acids by Coexpression of Trans-Anethole Oxygenase and p-Anisaldehyde Dehydrogenase Genes of *Pseudomonas Putida* JYR-1 in *Escherichia coli*. *J. Agric. Food Chem.* **2012**, *60*, 11972–11979.

(10) Senthamarai, T.; Chandrashekhar, V. G.; Rockstroh, N.; Rabeah, J.; Bartling, S.; Jagadeesh, R. V.; Beller, M. A “Universal” Catalyst for Aerobic Oxidations to Synthesize (Hetero) Aromatic Aldehydes, Ketones, Esters, Acids, Nitriles, and Amides. *Chem* **2022**, *8*, 508–531.

(11) Ma, Y.; Li, Z.; Zhang, H.; Wong, V. K. W.; Hollmann, F.; Wang, Y. Bionzymatic Cascade Combining a Peroxygenase with an Oxidase for the Synthesis of Aromatic Aldehydes from Benzyl Alcohols. *Catalysts* **2023**, *13*, No. 145.

(12) Urlacher, V. B.; Koschorreck, K. Peculiarities and Applications of Aryl-Alcohol Oxidases from Fungi. *Appl. Microbiol. Biotechnol.* **2021**, *105*, 4111–4126.

(13) Jankowski, N.; Koschorreck, K.; Urlacher, V. B. Aryl-Alcohol-Oxidase-Mediated Synthesis of Piperonal and Other Valuable Aldehydes. *Adv. Synth. Catal.* **2022**, *364*, 2364–2372.

(14) Klepach, H. M.; Zakalskiy, A. E.; Zakalska, O. M.; Gayda, G. Z.; Smutok, O.; Gonchar, M. V. Alcohol Oxidase from the Methylo-trophic Yeast *Ogataea Polymorpha*: Isolation, Purification, and Bioanalytical Application. *Methods Mol. Cell. Biol.* **2021**, 231–248.

(15) Viña-Gonzalez, J.; Elbl, K.; Ponte, X.; Valero, F.; Alcalde, M. Functional Expression of Aryl-alcohol Oxidase in *Saccharomyces Cerevisiae* and *Pichia Pastoris* by Directed Evolution. *Biotechnol. Bioeng.* **2018**, *115*, 1666–1674.

(16) Viña-Gonzalez, J.; Gonzalez-Perez, D.; Ferreira, P.; Martinez, A. T.; Alcalde, M. Focused Directed Evolution of Aryl-Alcohol Oxidase in *Saccharomyces Cerevisiae* by Using Chimeric Signal Peptides. *Appl. Environ. Microbiol.* **2015**, *81*, 6451–6462.

(17) Carro, J.; González-Benjumea, A.; Fernández-Fueyo, E.; Aranda, C.; Guallar, V.; Gutiérrez, A.; Martínez, A. T. Modulating Fatty Acid Epoxidation vs Hydroxylation in a Fungal Peroxygenase. *ACS Catal.* **2019**, *9*, 6234–6242.

(18) Ruiz-Dueñas, F. J.; Ferreira, P.; Martínez, M. J.; Martínez, A. T. In Vitro Activation, Purification, and Characterization of *Escherichia coli* Expressed Aryl-Alcohol Oxidase, a Unique H₂O₂-Producing Enzyme. *Protein Expression Purif.* **2006**, *45*, 191–199.

(19) Kato, N.; Omori, Y.; Tani, Y.; Ogata, K. Alcohol Oxidases of *Kloeckera* Sp. and *Hansenula Polymorpha*: Catalytic Properties and Subunit Structures. *Eur. J. Biochem.* **1976**, *64*, 341–350.

(20) Pickl, M.; Michael, F.; Silvia, M. G.; Kurt, F. The Substrate Tolerance of Alcohol Oxidases. *Appl. Microbiol. Biotechnol.* **2015**, *99*, 6617–6642.

(21) Nicholas, J. T. Enantioselective Oxidation of C–O and C–N Bonds Using Oxidases. *Chem. Rev.* **2011**, *111*, 4073–4087.

(22) Linke, D.; Lehnert, N.; Nimtz, M.; Berger, R. G. An Alcohol Oxidase of *Phanerochaete Chrysosporium* with a Distinct Glycerol Oxidase Activity. *Enzyme Microb. Technol.* **2014**, *61*–62, 7–12.

(23) Nguyen, Q.-T.; Romero, E.; Dijkman, W. P.; de Vasconcellos, S. P.; Binda, C.; Mattevi, A.; Fraaije, M. W. Structure-Based Engineering of *Phanerochaete Chrysosporium* Alcohol Oxidase for Enhanced Oxidative Power toward Glycerol. *Biochemistry* **2018**, *57*, 6209–6218.

(24) Martin, C.; Trajkovic, M.; Fraaije, M. W. Production of Hydroxy Acids: Selective Double Oxidation of Diols by Flavoprotein Alcohol Oxidase. *Angew. Chem., Int. Ed.* **2020**, *59*, 4869–4872.

(25) Hernández-Ortega, A.; Lucas, F.; Ferreira, P.; Medina, M.; Guallar, V.; Martínez, A. T. Role of Active Site Histidines in the Two Half-Reactions of the Aryl-Alcohol Oxidase Catalytic Cycle. *Biochemistry* **2012**, *51*, 6595–6608.

(26) Berendsen, H. J. C.; van der Spoel, D.; van Drunen, R. GROMACS: A Message-Passing Parallel Molecular Dynamics Implementation. *Comput. Phys. Commun.* **1995**, *91*, 43–56.

(27) The PLUMED consortium. Promoting Transparency and Reproducibility in Enhanced Molecular Simulations. *Nat. Methods* **2019**, *16*, 670–673.

(28) Valdés-Tresanco, M. S.; Valdés-Tresanco, M. E.; Valiente, P. A.; Moreno, E. Gmx_MMPBSA: A New Tool to Perform End-State Free Energy Calculations with GROMACS. *J. Chem. Theory Comput.* **2021**, *17*, 6281–6291.

(29) Onufriev, A.; Bashford, D.; Case, D. A. Exploring Protein Native States and Large-scale Conformational Changes with a Modified Generalized Born Model. *Proteins: Struct., Funct., Bioinf.* **2004**, *55*, 383–394.

(30) Kadowaki, M. A. S.; Higasi, P. M. R.; Godoy, M. O.; Araújo, E. A.; Godoy, A. S.; Prade, R. A.; IPolikarpov, G. Enzymatic versatility and thermostability of a new aryl-alcohol oxidase from *Thermothelomyces thermophilus* M77. *Biochim. Biophys. Acta, Gen. Subj.* **2020**, *1864*, No. 129681.

(31) Carro, J.; Martínez-Júlvez, M.; Medina, M.; Martínez, A. T.; Ferreira, P. Protein dynamics promote hydride tunnelling in substrate oxidation by aryl-alcohol oxidase. *Phys. Chem. Chem. Phys.* **2017**, *19*, 28666–28675.

(32) Romero, E.; Castellanos, J. R. G.; Gadda, G.; Fraaije, M. W.; Mattevi, A. Same Substrate, Many Reactions: Oxygen Activation in Flavoenzymes. *Chem. Rev.* **2018**, *118*, 1742–1769.

Recommended by ACS

Molecular Characterization of a Stereoselective and Promiscuous Flavanone 3-Hydroxylase from *Carthamus tinctorius* L

Songyang Sui, Lin Yang, *et al.*

JANUARY 12, 2023
JOURNAL OF AGRICULTURAL AND FOOD CHEMISTRY

READ 

Structural Insights into (Tere)phthalate-Ester Hydrolysis by a Carboxylesterase and Its Role in Promoting PET Depolymerization

Gerlis von Haugwitz, Ren Wei, *et al.*

NOVEMBER 29, 2022
ACS CATALYSIS

READ 

Directed Evolution of (R)-2-Hydroxyglutarate Dehydrogenase Improves 2-Oxoadipate Reduction by 2 Orders of Magnitude

Veronica Saez-Jimenez, Lisbeth Olsson, *et al.*

AUGUST 08, 2022
ACS SYNTHETIC BIOLOGY

READ 

Engineering a Prokaryotic Non-P450 Hydroxylase for 3'-Hydroxylation of Flavonoids

Hongyan Wang, Qipeng Yuan, *et al.*

NOVEMBER 02, 2022
ACS SYNTHETIC BIOLOGY

READ 

Get More Suggestions >